Results in Physics 10 (2018) 434–443

Contents lists available at ScienceDirect

Results in Physics

journal homepage: www.elsevier.com/locate/rinp

Fabrication and comparative study of magnetic Fe and α-Fe_2O_3 nanoparticles dispersed hybrid polymer (PVA + Chitosan) novel nanocomposite film

Md. Asadul Hoque[a], M.R. Ahmed[a], G.T. Rahman[a], M.T. Rahman[a], M.A. Islam[a], Mubarak A. Khan[b], M. Khalid Hossain[b,*]

[a] Dept of Materials Science & Engineering, University of Rajshahi, Rajshahi 6205, Bangladesh
[b] Atomic Energy Research Establishment, Bangladesh Atomic Energy Commission, Dhaka 1349, Bangladesh

ARTICLE INFO

Keywords:
Magnetic nanoparticles
Sol-gel and chemical reduction method
Biodegradable polymer
Biocompatible nanocomposite
Mechanical properties
Biomedical applications

ABSTRACT

Incorporation of nanoparticles into polymer matrix allows the development of new features that differs from the pure materials. In this research, magnetic nanoparticles reinforced organic biodegradable polymer matrix based biocompatible nanocomposite films were fabricated. This work covered, synthesis of Iron (Fe) and Iron oxide (α-Fe_2O_3) nanoparticles by chemical reduction and sol-gel method respectively, fabrication of Fe/Polyvinyl alcohol (PVA)/Chitosan and α-Fe_2O_3/PVA/Chitosan nanocomposites by solvent casting method, and evaluation and comparison of their mechanical properties to find the superior biocompatible nanocomposite. The X-ray diffraction (XRD), scanning electron microscopy (SEM), and energy dispersive spectroscopy (EDX) analysis confirmed the size, structure, morphology and formation of Fe and α-Fe_2O_3 nanoparticles. Magnetic study showed that, synthesized α-Fe_2O_3 nanoparticle possess better magnetic properties than the Fe nanoparticle. The Fourier-transform infrared spectroscopy (FTIR) spectra confirmed the successful interaction of Fe and α-Fe_2O_3 nanoparticles with the polymer matrix. The Iron oxide dispersed (16.67 wt%) nanocomposite α-Fe_2O_3/PVA/Chitosan showed highest tensile strength and elastic modulus that is respectively 45% and 40% higher than the PVA polymer alone. This novel nanocomposite may potentially be useful in various biomedical applications.

Introduction

Magnetic nanoparticles (NPs) have gained considerable attention due to its unique properties over bulk materials and easy controllability by magnetic field [1]. For instance, magnetic iron (Fe) nanoparticles have a huge potential for biomedical applications including drug delivery, cell labeling, hyperthermia treatments and MRI contrast agents [2]. Among the other iron oxides, hematite (α-Fe_2O_3) is most stable and popular candidate because of its excellent corrosion resistance, cheap production coast, biocompatibility, eco-friendly as well as non-toxicity properties [3,4]. Besides this, hematite nanoparticle has extensive surface to-volume ratio, therefore they possess high surface energies [5]. To take the advantage of these significant properties, nanoparticles can be reinforced into polymer matrices to increase their application along with physio-chemical properties [6,7].

Polyvinyl alcohol (PVA) has been widely utilized in biomedical applications such as drug delivery systems, contact lenses, artificial heart surgery, and wound dressings [8], cartilage replacements [9], surgical threads [10], owing to its specific properties such as non-toxicity, variety of molecular weights, high oxygen permeability, biodegradability and good interactions with metal oxide nanoparticles [11–15]. However, PVA possess very less mechanical strength. To overcome this major drawback, it should be chemically cross-linked/blended with other hydrophilic materials to induce mechanical stability. Chitosan is composed of 2-amino-2-deoxy-β-d-glucan, a linear polysaccharide can be dissolved easily in water [16]. Amino groups of Chitosan provide a hydrophilic environment compatible with the biomolecules. Also, modification of pendants on chitosan provides significant advantages in biomedical applications, as for instance biosensors [17], hyperthermia treatment, tissue engineering [1,18,19], enzymatic assays [20], drug delivery [21], magnetic resonance imaging (MRI) [22], cell separation [23], and clinical diagnostics because of their biodegradability and good biocompatibility. Among the various hydrophilic biopolymers, Chitosan has biocompatibility, excellent film-forming ability, high chemical modification responsivity, non-toxicity, high water permeability, cost-effectiveness etc. [17]. In order to

* Corresponding author.
E-mail address: khalid.baec@gmail.com (M.K. Hossain).

https://doi.org/10.1016/j.rinp.2018.06.010
Received 17 May 2018; Received in revised form 4 June 2018; Accepted 5 June 2018
Available online 15 June 2018

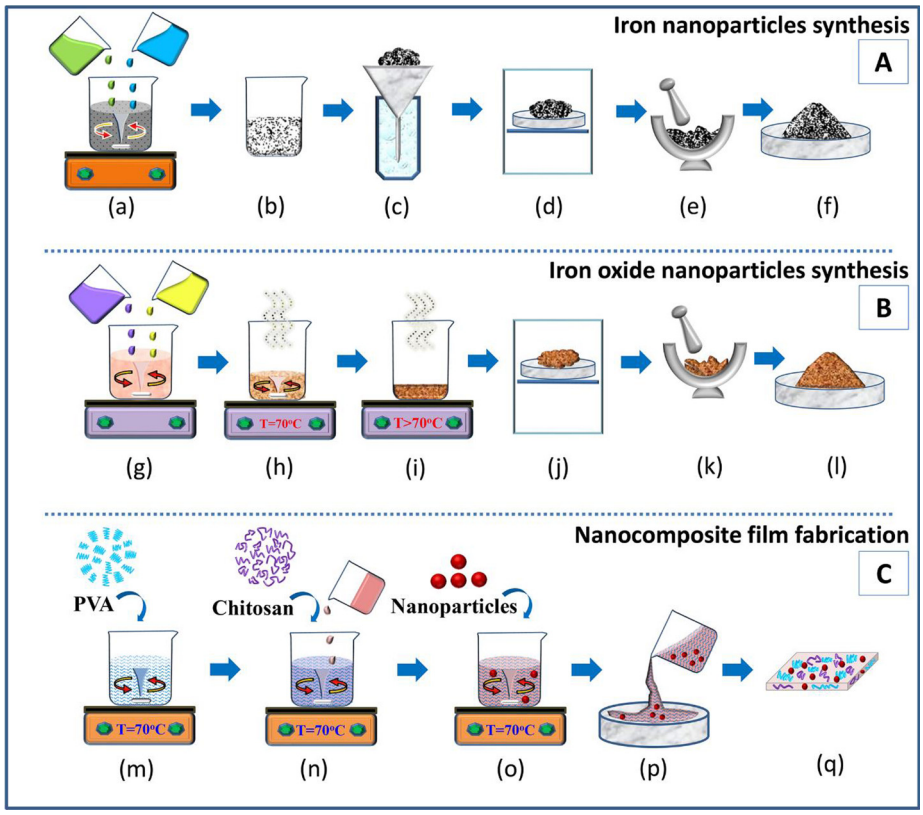

Fig. 1. (A) Schematic presentation of synthesis of Iron nanoparticles by chemical reduction method: (a) drop wise mixing of ferric chloride hydrate and sodium borohydride solution, (b) formation of black powder, (c) filtration of produced product, (d) vacuum oven drying, (e) grinding of the obtained product, and (f) synthesized Fe nanoparticles. (B) Schematic presentation of synthesis of Iron oxide nanoparticles by sol-gel method: (g) drop wise mixing of iron nitrate and hydrated citric acid solution at 70 °C, (h) formation of Iron oxide gel, (i) drying to remove solution, (j) annealing of the produced product, (k) grinding of the obtained product, and (l) synthesized α-Fe_2O_3 nanoparticles. (C) Schematic presentation of fabrication of polymer blended nanocomposite films by solvent casting method: (m) dissolution of PVA, (n) dissolution of Chitosan in addition of acetic acid, (o) addition of nanoparticles, (p) drying and casting into glass frame, and (q) fabricated polymer nanocomposite film.

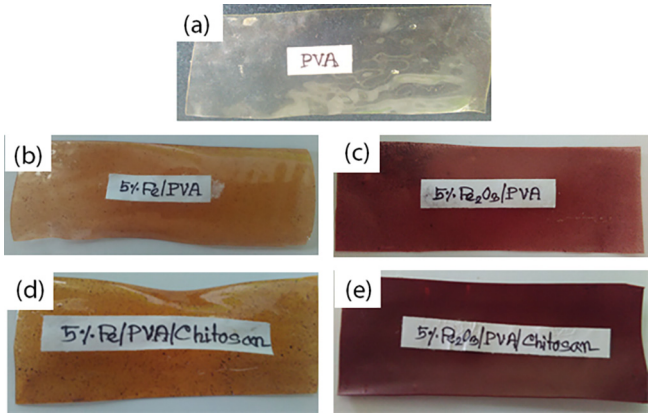

Fig. 2. Nanocomposite films from (a) PVA, (b) Fe/PVA, (c) α-Fe_2O_3/PVA, (d) Fe/PVA/Chitosan, and (e) α-Fe_2O_3/PVA/Chitosan.

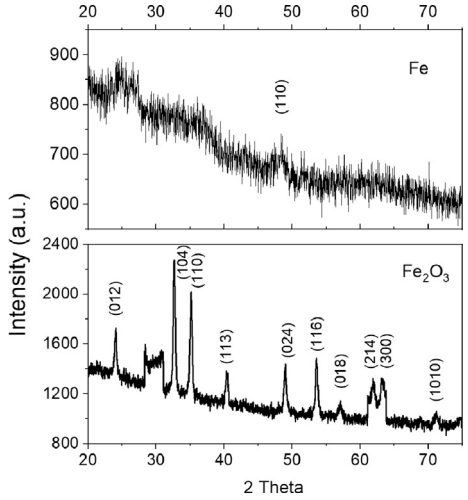

Fig. 3. XRD patterns of (a) Fe and (b) α-Fe_2O_3 nanoparticles.

improve mechanical properties of both PVA and Chitosan polymers, they could be blended/chemically crosslinked for obtaining flexible and mechanically stable composite material.

Generally, the reinforcement of nano-particles into the polymer matrix enhances the mechanical, dimensional and thermal stabilities of the host polymer matrix. In previous studies, α-Fe_2O_3/(PVA + PEG) composites were fabricated to investigate optical and electrical properties [24], α-Fe_2O_3/Chitosan composites were fabricated to investigate antibacterial activity [25], α-Fe_2O_3/Chitosan composites were fabricated to investigate dye decolourization properties [26], Fe_2O_3/PVA composites were fabricated to investigate thermal properties [27], Fe_3O_4/Chitosan/PVA fibers were fabricated to investigate electrical, mechanical, and magnetic properties [28], and Fe_2O_3/PAN composites were fabricated to investigate optical properties [29]. According to previous reports, most work in this field has been done to fabricate Fe_2O_3 dispersed PVA or Chitosan individually. Also, less importance was given to evaluate the mechanical properties. Therefore, the main objective of this work is to fabricate novel natural (Chitosan)-synthetic (PVA) hybrid polymer matrix nanocomposites using magnetic Fe and α-Fe_2O_3 nanoparticles as reinforcement. According to the advantages and scopes discussed above, these newly fabricated composites could be used in biomedical sectors.

In this work, the magnetic Fe and α-Fe_2O_3 were synthesized by chemical reduction method and sol-gel method respectively. The synthesized nanoparticles were investigated with XRD, SEM, EDS and impedance analyzer to determine their structural, morphological, compositional, and magnetic properties respectively. Then, Fe nanoparticles dispersed Fe/PVA, Fe/PVA/Chitosan as well as α-Fe_2O_3 nanoparticles dispersed α-Fe_2O_3/PVA, α-Fe_2O_3/PVA/Chitosan hybrid polymer nanocomposites were fabricated by solvent casting method.

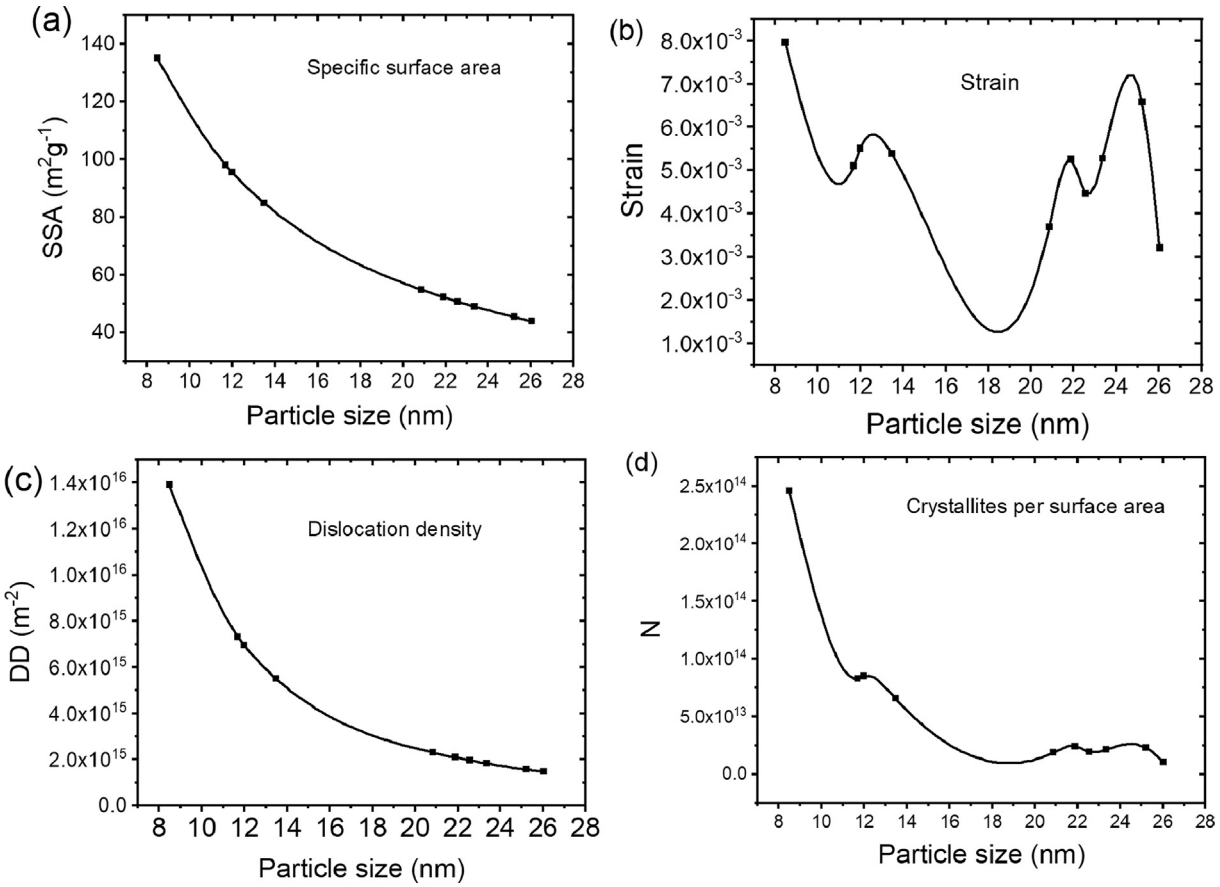

Fig. 4. Variation of α-Fe_2O_3 nanoparticle sizes with (a) specific surface area (SSA), (b) lattice strain, (c) dislocation density (DD), and (d) crystallites/surface area (N).

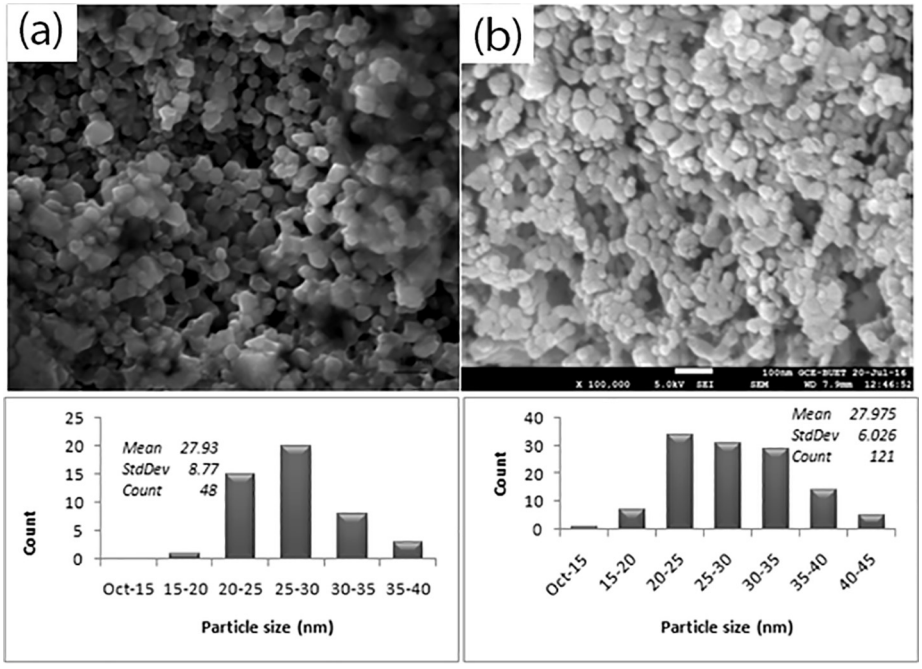

Fig. 5. SEM pictures of (a) iron (Fe) and (b) iron oxide (α-Fe_2O_3) nanoparticles with corresponding particle size distribution chart.

FTIR analysis was done to investigate the binding nature of nanoparticles with PVA and Chitosan matrix. Additionally, tensile test was carried out to make a comparative statement on the mechanical properties such as tensile strength, elongation and elastic modulus of the fabricated novel nanocomposites.

Materials and methods

Materials

Ferric chloride hydrate (≥98%) was purchased from Loba

Table 1
Nanoparticle sizes from XRD and SEM analysis.

Nanoparticle types	XRD calculation	SEM measurement
Fe nanoparticles	8.305 nm	27.929 nm
α-Fe_2O_3 nanoparticles	18.55 nm	27.975 nm

Chemicals, India, Sodium borohydride (≥95%), Iron nitrate (≥98%), Citric acid (≥99.5%), Polyvinyl alcohol (≥98%), Acetic acid (1M) were purchased from Merck, India, and Chitosan, $(C_6H_{11}NO_4)_n$ was supplied by Institution of Radiation and Polymer Technology (IRPT), Bangladesh Atomic Energy Commission. All chemicals were used as received.

Synthesis of iron (Fe) nanoparticles

Two different solution were used to synthesize Iron nanoparticle following chemical reduction method [30], as illustrated in Fig. 1(a)–(f). For one solution, 1.35 g of hydrated ferric chloride ($FeCl_3{\cdot}6H_2O$, ≥98%) was dissolved into 40 ml deionized water. For other solution, 0.95 g of sodium borohydride ($NaBH_4$, ≥95%) was

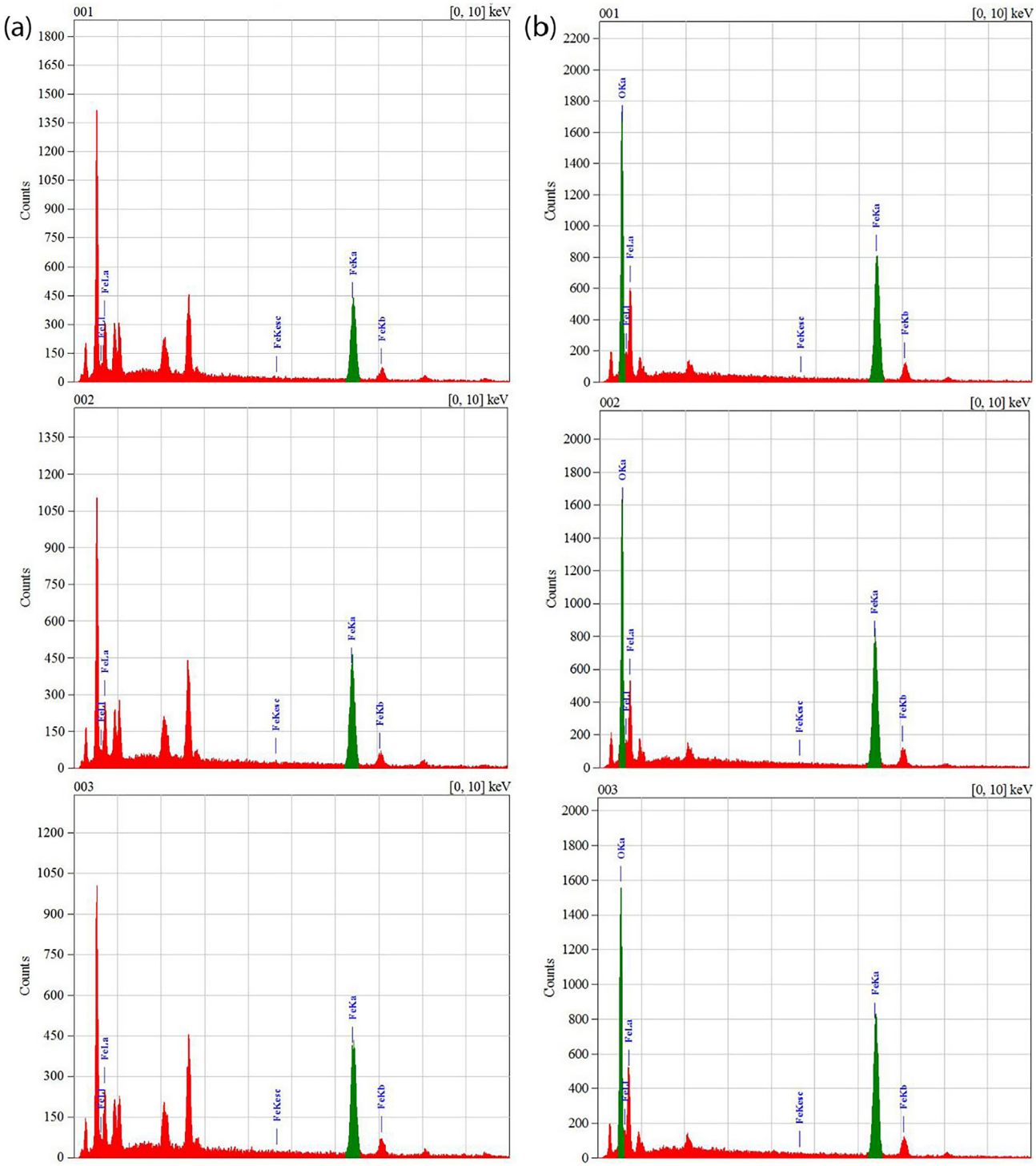

Fig. 6. EDS spectrum and distribution of element for (a) Iron (Fe) nanoparticles, and (b) Iron oxide (Fe_2O_3) nanoparticles.

Table 2
Comparison of atomic mass percentage for Fe and α-Fe_2O_3 obtained from EDS with theoretical values.

Nanoparticle sample	Elements	Atomic mass percentage (%) from EDX spectra				Theoretical value
		Point 1	Point 2	Point 3	Average	
Fe	Fe	100	100	100	100	100
α-Fe_2O_3	Fe O	67.48 32.52	68.74 31.26	67.95 32.05	68.06 31.94	70 30

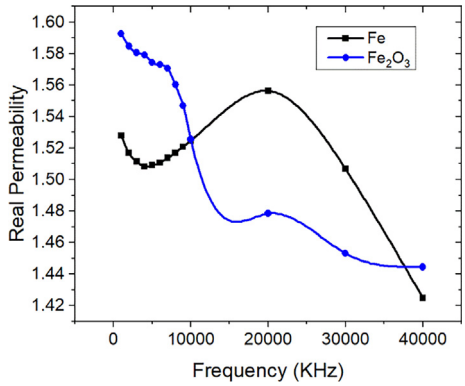

Fig. 7. Frequency dependent real permeability of iron and iron oxide nanoparticles.

Table 3
Characteristic absorption of Iron, Iron oxide nanoparticles, PVA, Chitosan matrix.

Absorbing group	Absorption position
Characteristic Absoption of Nanoparticles	
Iron nanoparticles	478.06 cm^{-1}, 562.10 cm^{-1} and 693.68 cm^{-1}
Hematite (Fe_2O_3)	523.78 cm^{-1} and 436.21 cm^{-1}
Characteristic Absoption of PVA	
Stretching vibration of O–H absorption	3272.45 cm^{-1}
Asymmetric stretching of C—H	2922.48 cm^{-1}
Symmetric stretching of C—H	2853.92 cm^{-1}
Characteristic Absoption of Chitosan	
Stretching vibration of amino group	1377.89 cm^{-1}, 3274.87 cm^{-1}
Stretching of C—H	2920.79 cm^{-1}

dissolved into 10 ml deionized water. Then both solutions were mixed up drop wise, while maintaining vigorous stirring by magnetic stirrer. During mixing, instantaneously (less than 1 s) black powder was produced. At the end of the reaction, through filtration process produced particles were isolated from the solution. The filtered product was then dried in vacuum oven. Later, the product was grinded to get light reddish brown Fe nanoparticles powder.

Synthesis of iron oxide (α-Fe_2O_3) nanoparticles

The magnetic Iron oxide nanoparticle was synthesized by the sol-gel method [31–34], as illustrated in Fig. 1(g)–(l). As a precursor solution, 200 ml (0.1 M) of iron nitrate (Fe $(NO_3)_3{\cdot}9H_2O$, ≥98%) was used and gelated by addition of 800 ml (0.1 M) of mono hydrated citric acid ($C_6H_8O_7{\cdot}H_2O$, ≥99.5) solution as ligand molecules, and distilled water as the solvent. The iron salt solution was mixed drop wise to the citric acid solution, while the solution stirred vigorously. After mixing, the temperature of the solution was raised up to 70 °C, vigorous stirring was maintained until the gel was formed. Later, temperature was increased to evaporate the remaining water for drying the gel and the dried gel was annealed at temperature of 300 °C. After drying, the powder was grinded by mortar and pestle, typically yielding 1.5 g of dark reddish brown Fe_2O_3 nanoparticles.

Fabrication of nanodispersed polymer composite films

Nanocomposite films were fabricated by solvent casting method, as illustrated in Fig. 1(m)–(q). At first, 7 gm PVA was dissolved in 100 ml deionized water at 70 °C with vigorous stirring. After that, in the solution 3 gm chitosan was added while maintaining vigorous stirring without changing the temperature. To assist the solubility of chitosan in water, 2 ml 1 M Acetic acid was added to the mixture. When chitosan was dissolved completely, nanoparticles (Fe or α-Fe_2O_3) were added in the liquid polymer blend to ensure proper mixing. Finally, removing the air bubbles, produced during stirring, the mixture was cast into a silica paper covered flat glass mold and dried overnight using dehumidifier. Fabricated film thickness (0.4 mm) was measured using Digital Vernier Caliper (Mitutoyo, Series: 500, Japan). Because of the high aspect ratio of the nanoparticles, the concentration (wt.%) of the nanoparticles in the fabricated composite were selected to be 2%, 5%, 9% and 16.67% respectively. Fabricated nanocomposite films from PVA, Fe/PVA, α-Fe_2O_3/PVA, Fe/PVA/Chitosan, and α-Fe_2O_3/PVA/Chitosan are shown in Fig. 2.

Materials characterization

Phase analysis was carried out using EMMA XRD-6000 X-ray diffractometer which was equipped with Ni-filtered CuKα radiation (λ = 1.5406 Å). The diffractometer was operated with 2° diverging and receiving slits at 50 kV and 40 mA. A continuous scan was carried out with a step size of 0.02° and a step time of 0.2 s. From XRD peaks, the particle size of both Fe and α-Fe_2O_3 was calculated using Debye-Sherrer equation [35–38]. The surface morphology of the nanoparticle was observed using SEM (HITACHI S-3400N), operated at 5 kV. The particle size of both Fe and α-Fe_2O_3 was also calculated from SEM image using ImageJ software [39]. EDS was used for elemental analysis. The distribution of element on the materials surface was also analyzed. The same sample, used for SEM, was investigated using EDS. The chemical composition and the metal-polymer bonding nature were confirmed by analyzing FTIR spectra. For taking FTIR peaks using Perkin Elmer Frontier FTIR Spectrometer, fabricated samples were placed onto a zinc selenide crystal, and the analysis was performed within the spectral region of 400–4000 cm^{-1} with 64 scans recorded at a 4 cm^{-1} resolution. The data was then analyzed using *Perking Elmer Spectrum* software. The impedance of the toroid shaped samples at room temperature was measured with the Hewlett Packard (4291A) Impedance Analyzer in the frequency range 1 kHz to 120 MHz. From these data, frequency dependent real permeability was calculated. The produced Fe/PVA/Chitosan and α-Fe_2O_3/PVA/Chitosan nanocomposite films were carefully cut into rectangles (8 × 2 $in.^2$) and mechanical properties such as tensile strength, elastic modulus, and elongation of the composite films were measured using Universal Testing Machine TINIUS OLSEN H50KS (TX1091) with an approach speed of 20 mm/min with 20 mm gauze length.

Results and discussion

XRD studies of Fe and α-Fe_2O_3 nanoparticles

The crystal structure and the phase composition of the produced iron and iron oxide nanoparticles were identified by XRD powder analysis. Fig. 3 shows the XRD patterns of synthesized iron and iron oxide nanoparticles respectively. Although the peaks of iron nanoparticles were not sharp, a broadened peak was observed at 48.34°. The corresponding crystal plane and d-spacing were found (1 1 0) and

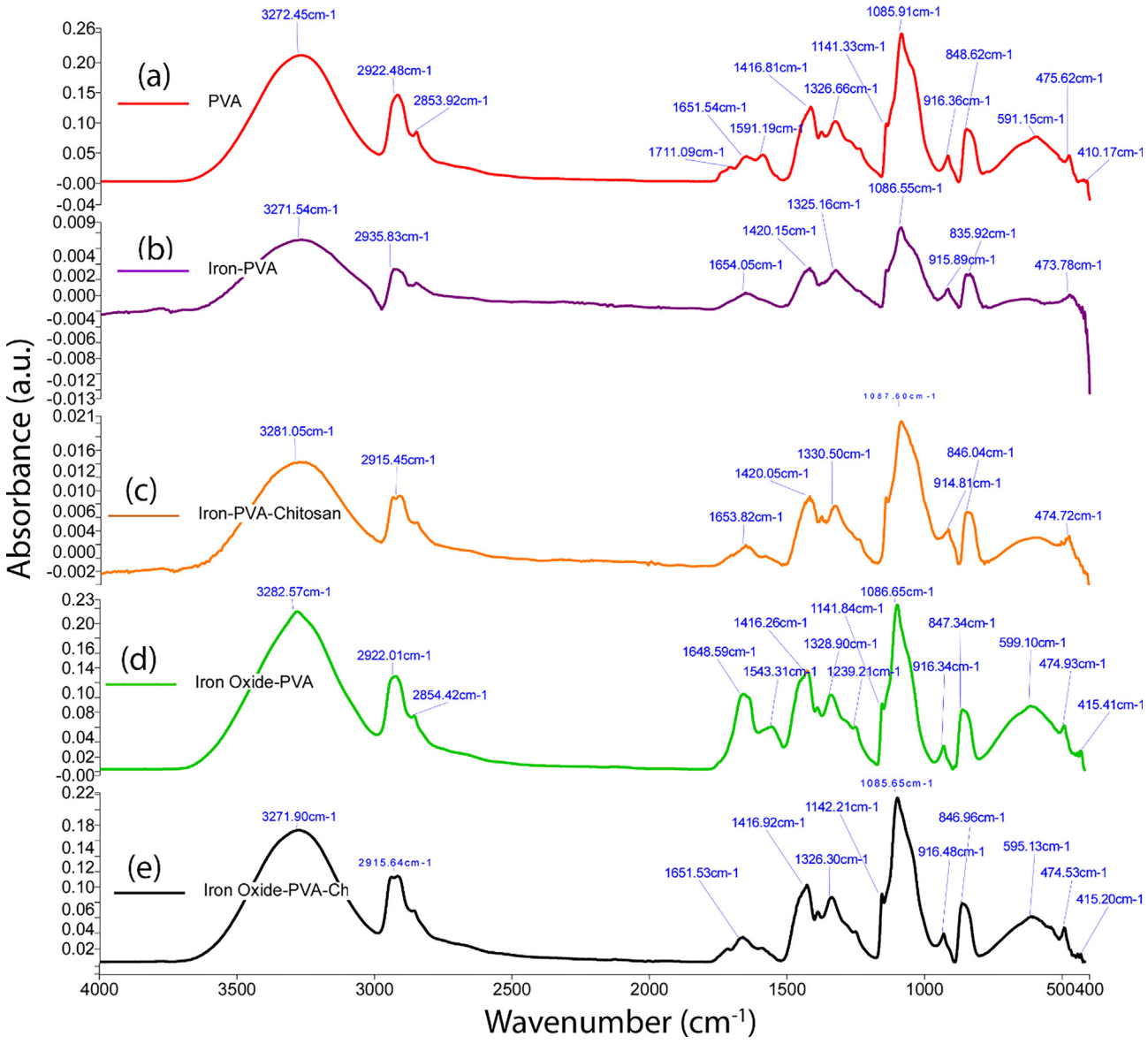

Fig. 8. FTIR spectra of (a) PVA, (b) Iron/PVA, (c) Iron/PVA/Chitosan, (d) Iron oxide/PVA, and (e) Iron oxide/PVA/Chitosan.

0.19 nm respectively. This indicates that the produced light reddish brown powder is cubic α-Fe [30,40,41]. The iron oxide nanoparticles have common peak at 24.12° (0 1 2), 32.66° (1 0 4), 35.12° (1 1 0), 40.36° (1 1 3), 49.02° (0 2 4), 53.56° (1 1 6), 57.1° (0 1 8), 61.86° (2 1 4), 63.32° (3 0 0) and 71.18° (1010). The calculated *d*-spacings are 0.37, 0.27, 0.26, 0.22, 0.19, 0.17, 0.16, 0.15, 0.15 and 0.13 nm respectively which are in agreement with those of the standard XRD pattern of α-Fe_2O_3 [42]. This confirms that the synthesized dark reddish-brown iron oxide nanoparticles are hexagonal hematite (α-Fe_2O_3) phase [43,44]. The particles size of Fe was found to be 8.31 nm as well as for α-Fe_2O_3 it was ranged from 8.47 nm to 26.06 nm with an average of 18.55 nm. The Fig. 4(a) shows the variation of specific surface area (SSA) with α-Fe_2O_3 particle size and it is seen that, SSA increases dramatically as the size of materials decreases and small sizes particles have high chemical reactivity than the larger one. The variation of lattice strain with α-Fe_2O_3 particle size is shown in Fig. 4(b). It is seen that, the lattice strain changes abruptly with particle size. Dislocation density with α-Fe_2O_3 particles size plotted in Fig. 4(c) shows that dislocation density (DD) increases while particle size decreases. It implies that the prepared Fe_2O_3 nanoparticles have more strength and hardness than their bulk (Fe_2O_3) counterpart [45]. The variation of crystallites/surface area (N) with α-Fe_2O_3 particle size is illustrated in Fig. 4(d). It is seen that, the crystallites/surface area increases as particle size decreases.

SEM analysis

Scanning electron microscopy (SEM) analysis was used to confirm the morphology and sizes of the synthesized iron and iron oxide samples. The Fig. 5(a) shows the image of iron with particle size distribution chart. The obtained results clearly show that the iron nanoparticles have spherical shape. Although some particles are agglomerated, most of the particles can be identified by nanometer scale. The average size of Fe nanoparticles calculated from SEM images, were found to be 27.93 nm with standard deviation 8.77 (minimum size = 18.61 nm, maximum size = 39.38 nm). The SEM picture of iron oxide (α-Fe_2O_3) is shown in Fig. 5(b), which reveals the formation of the nanoparticles with spherical-shaped. Although there are some agglomeration of α-Fe_2O_3 nanoparticles in some areas the average particles size were calculated as 27.98 nm with standard deviation 6.03 (minimum size = 14.57 nm, maximum size = 42.69 nm). Table 1 represents the variation in particle size calculated from XRD and SEM data.

Table 4
Tensile properties of Fe and α-Fe_2O_3 nanoparticles dispersed PVA and PVA/Chitosan nanocomposite films.

No.	Nanoparticle concentration (wt.%)	Sample name	Tensile strength (MPa)	Elastic modulus (MPa)	Elongation (%)
1		PVA	8.35	32.56	242.5
2	2%	Fe/PVA Fe/PVA/Chitosan	6.48 7.08	29.15 21.60	116.1 114.3
3	5%	Fe/PVA Fe/PVA/Chitosan	6.82 7.69	31.26 23.53	112.4 116.8
4	9%	Fe/PVA Fe/PVA/Chitosan	7.29 8.19	34.47 28.84	106.2 101.7
5	16.7%	Fe/PVA Fe/PVA/Chitosan	7.78 8.83	38.54 35.59	98.7 92.8
6	2%	Fe_2O_3/PVA Fe_2O_3/PVA/Chitosan	6.92 9.67	31.25 33.67	200.0 198.6
7	5%	Fe_2O_3/PVA Fe_2O_3/PVA/Chitosan	7.69 10.98	33.55 38.46	196.0 194.8
8	9%	Fe_2O_3/PVA Fe_2O_3/PVA/Chitosan	7.94 11.24	37.56 41.78	155.3 174.6
9	16.7%	Fe_2O_3/PVA Fe_2O_3/PVA/Chitosan	8.46 12.15	41.87 45.69	124.8 156.8

EDS analysis

The EDS graphs of synthesized iron and iron oxide nanoparticles are shown in Fig. 6. Table 2 shows the summarized atomic mass percentage of Fe or Fe and O obtained from EDX spectra of Fe and α-Fe_2O_3 nanoparticles with comparison of their theoretical values. The kinetic energy of the emitted electrons for iron (Fe) atom energy is 6.398 keV and for oxygen atom (O) 0.525 keV. Thus, EDS spectrum at Fig. 6(a) indicates the sample contains 100% iron (Fe). On the other hand, the Fig. 6(b) shows that, the average atomic mass percentage of sample are 68.06% Fe and 31.94% O, which is in good agreement with those of the theoretical values of 70% Fe and 30% O in α-Fe_2O_3 compound. Thus, from the investigation, it is clear that the produced nano-sized particles were α-Fe_2O_3.

Evaluation of magnetic properties

The produced dark brown reddish iron oxide nanoparticles, strongly attracted on magnetic bar, are paramagnetic in nature [46]. Fig. 7 represents the frequency dependent real permeability [47] of synthesized Fe and α-Fe_2O_3 nanoparticles in the frequency range of 1 kHz to 40 MHz at 0.5 Volt and 30 °C. It was seen that the real permeability of iron nanoparticles decreased upon increasing frequency till the value reached at 6000 kHz. After that the permeability increased with increasing frequency until 20 MHz and then started to decrease. For iron oxide nanoparticles, permeability decreased gradually with increasing frequency. Flat profile at high frequency indicates that Fe and α-Fe_2O_3 nanoparticles have good high frequency stability.

FTIR analysis

Characteristic absorption of Iron, Iron oxide nanoparticles, PVA and Chitosan matrix have been tabulated in the Table 3. Also, FTIR spectra of PVA, Fe/PVA, Fe/PVA/Chitosan, α-Fe_2O_3/PVA and α-Fe_2O_3/PVA/Chitosan are shown in Fig. 8. The characteristic absorption bands of PVA occurred at 3272.45 cm^{-1} is assignable to the stretching vibration of O—H absorption, 2922.48 cm^{-1} is assignable to asymmetric stretching of C—H, 2853.92 cm^{-1} is symmetric stretching of C—H [48,49]. The characteristic absorptions of the chitosan are at 2920.79 cm^{-1} and 3274.87 cm^{-1} are assignable to the C—H and N—H absorption respectively [50].

From the IR spectra of Fe/PVA and Fe_2O_3/PVA nanocomposites, all the absorption peaks of PVA are found and noticeably it is seen that characteristic peak of OH stretching was shifted from 3272.45 cm^{-1} to 3282.57 cm^{-1} indicating the interactions of Fe or Fe_2O_3 with the PVA matrix in the composites.

But when Chitosan was added to Fe_2O_3/PVA forming Fe_2O_3/PVA/Chitosan composite, the OH absorption peak of PVA again shifted at lower frequency (3271.90 cm^{-1}) indicating the mutual interaction of OH of PVA, Fe_2O_3 and NH group of chitosan. The characteristic absorption peak of iron and iron oxide can not be seen in the FTIR spectra of Fe/PVA/Chitosan and α-Fe_2O_3/PVA/Chitosan composites films. This is probably due to the presence of low percentage content of nanoparticles in the composites. Again, the nanoparticles were ingrained in the PVA and Chitosan matrix which could suppress the absorption band of Iron and Iron oxide resulting the missing of characteristic IR absorption of the nanoparticles in composites.

Mechanical properties of the films

Tensile properties of fabricated PVA nanoparticles/PVA and nanoparticles/PVA/Chitosan composites with different Fe and α-Fe_2O_3 loadings are tabulated in Table 4 and the representative graphs are illustrated in Fig. 9. According to the Fig. 9(a) and (b) it is clear that, due to incorporation of Fe and α-Fe_2O_3 nanoparticles in PVA matrix, both the tensile strength and elongation were decreased as compared to mere PVA film. It is also seen that, upon increasing the concentration of nanoparticles, the tensile strength increased slightly. Increase of nanoparticles concentration influenced on rigidity of nanocomposites, thus, they become more rigid due to addition of more nanoparticles [51] resulting in slight increase of the tensile strength. Also, the aggregation of nanoparticles became less effective to the localized variation of film thickness. On the other hand, the elastic modulus of the films was increased with increasing nanoparticles concentration [52] as shown in the Fig. 9(c).

The mechanical properties of polymer nanocomposite depend on the interaction between the matrix and the fillers [53]. Nanocomposites fabricated from various polymers and nanoparticles do not always exhibit improved tensile strength. Sometimes, agglomeration of nanoparticles inside the polymer matrices becomes responsible for decreasing the tensile strength. This implies that the interfacial bonding between matrix and particle is not strong enough to bear large mechanical stress, as because of inhomogeneous dispersion of nanoparticles [53]. The presence of highly stiff Fe and α-Fe_2O_3 nanoparticles in polymer matrix is responsible for enhancing the elastic modulus and lowering the elongation of the polymer. Generally, with increment of load the material tend to deform. But the deformation can be resisted by incorporating nanomaterials in the matrix. Because of having high surface energy as well as high surface area to volume fraction, nanoparticles easily interact with the matrix material by forming bond. Additionally, due to their nano size they can easily fill the intermolecular space into polymer matrix. In this way, the movement of dislocations becomes suppressed that makes the material brittle and hard. Thus, presence of nanomaterials in polymer matrix resists the deformation. Therefore, the composite can bear more loads, resulting higher elastic modulus and lower elongation compared with pure polymer alone.

Most significantly, the nanoparticles/PVA/Chitosan films showed better tensile strength, elongation and elastic modulus compared with

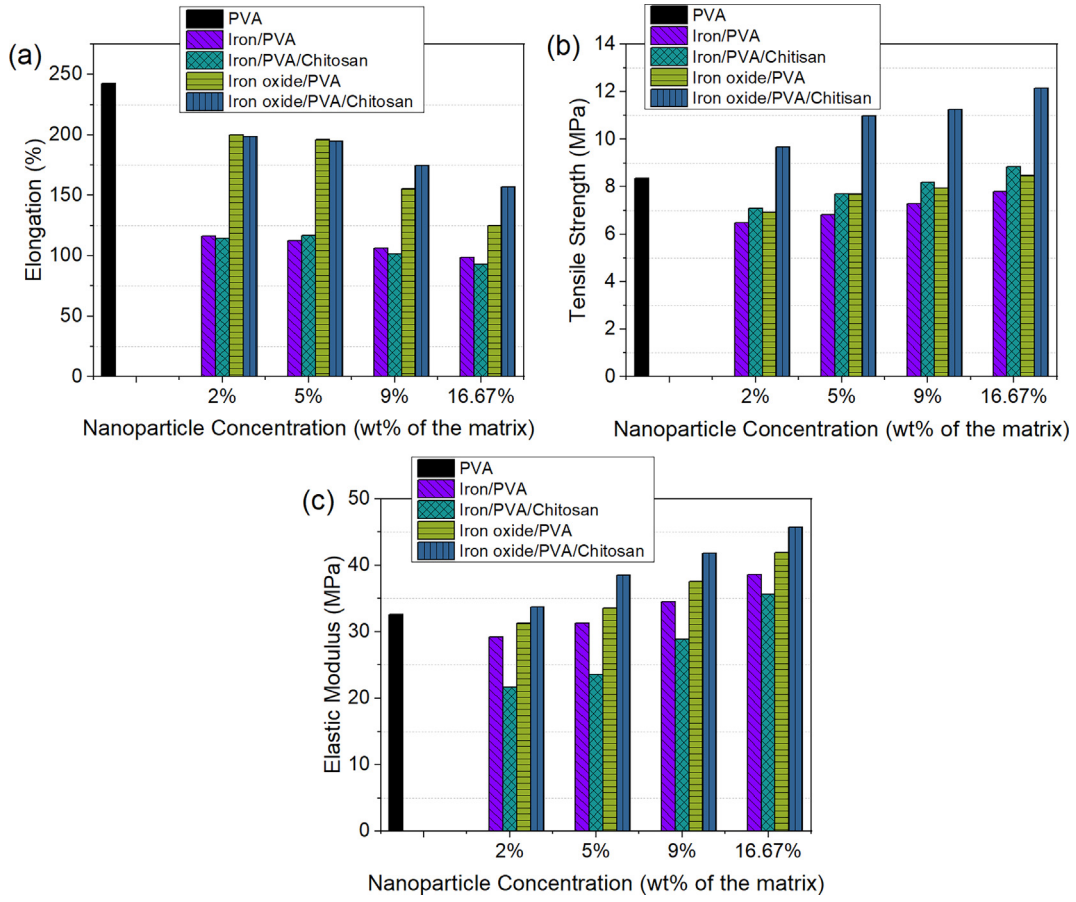

Fig. 9. Variation of (a) tensile strength, (b) elongation and (c) elastic modulus with nanoparticle concentration of the produced nanocomposite films.

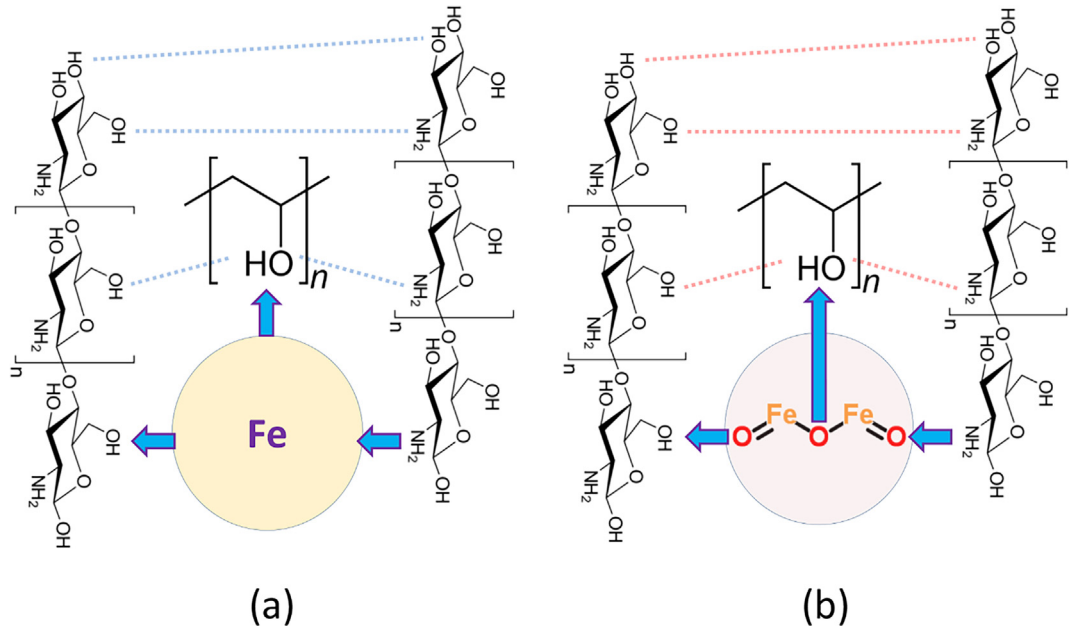

Fig. 10. Schematic illustration for the interactions in (a) Fe/PVA/Chitosan and (b) α-Fe_2O_3/PVA/Chitosan nanocomposite.

the nanoparticles/PVA films. From the Fig. 9(a)–(c) it is also seen that in presence of chitosan tensile strength and elastic modulus shows higher values than pure PVA polymer. Chitosan, as a stabilizing agent with its mechanical strength, excellent film-forming ability and bridging role between the metal/metal oxide reinforcement and PVA matrix contributes to the higher mechanical performances as compared to that of nanoparticles reinforced composites without Chitosan. Among Fe/PVA/Chitosan films and α-Fe_2O_3/PVA/Chitosan films, the later one showed better mechanical properties and it is due to the greater electrostatic interaction between the oxide group of α-Fe_2O_3 and amino functional chitosan molecules [54]. The improved mechanical properties are also due to the formation of polymer crosslinking i.e.

interaction between PVA–Chitosan polymer chains. The mechanical test confirms the superior properties of fabricated α-Fe_2O_3/PVA/Chitosan composite, on that account; these composites can be used successfully in biomedical sectors.

The possible interactions among the functional groups presented in fabricated polymer nanocomposites are illustrated in Fig. 10(a) and (b) for Fe/PVA/Chitosan and α-Fe_2O_3/PVA/Chitosan respectively. It can be assumed from in the Fig. 10(a) that, Fe might contribute electrons to electronegative oxygen of the hydroxy groups of the both PVA and Chitosan resulting partial positive charge to the Fe (as $Fe\delta^+$). The developed positive charged $Fe\delta^+$ might be compensated by the sharing of lone pair electrons of nitrogen ($-NH_2$) of the chitosan. On the other hand, the other possible hydrogen bonding among the hydroxyl-hydroxyl and hydroxyl-amino groups of PVA and Chitosan chains. The overall mechanism ultimately creates a bonding network in the Fe/PVA/Chitosan composite. For the α-Fe_2O_3/PVA/Chitosan composite, Fig. 10(b) illustrate that the hydrogen bonding among the oxygen of Fe_2O_3 and hydroxyl hydrogen of PVA and chitosan dominate the bonding network. All other the interactions of Fe/PVA/Chitosan composite (as shown in Fig. 10(a) also prevail in the α-Fe_2O_3/PVA/Chitosan composite. The overall mechanism ultimately creates a bonding network in the α-Fe_2O_3/PVA/Chitosan composite. As a result, it is expected to have improved dimensional and mechanical properties in fabricated nanocomposites. Comparing to the two composites, α-Fe_2O_3/PVA/Chitosan might have stronger bonding strength compare to that of the Fe/PVA/Chitosan composite which ultimately predict that α-Fe_2O_3/PVA/Chitosan should have better dimensional stability and mechanical properties.

Conclusion

In this study, the iron and iron oxide nanoparticles were synthesized by chemical reduction method and sol-gel method respectively. These synthesized nanoparticles were dispersed (2–16.67 wt%) into synthetic PVA and natural chitosan polymer matrix to fabricate novel nanocomposites such as Fe/PVA/Chitosan and α-Fe_2O_3/PVA/Chitosan by solvent casting method. XRD patterns of the synthesized nanoparticles confirmed the production of cubic Fe nanoparticles and hexagonal α-Fe_2O_3 nanoparticles with average diameter of 8.31 nm and 18.55 nm respectively. On the contrary, SEM images of the nanoparticles showed relatively larger particle sizes of average diameter of 27.93 nm for Fe and 27.98 nm for α-Fe_2O_3 nanoparticles. From SEM image, it was confirmed that the produced nanoparticles have spherical morphology with some agglomeration. The EDS spectrum also indicates the formation of pure Fe and α-Fe_2O_3 nanoparticles. From the impedance analyzer analysis, it was seen that iron and iron oxide nanoparticles have high frequency stability. For all concentration of the nanoparticles loading, α-Fe_2O_3/PVA/Chitosan nanocomposite films showed better tensile strength, elongation and elastic modulus than that of Fe/PVA/Chitosan films. Therefore, fabricated novel α-Fe_2O_3/PVA/Chitosan nanocomposite would be potential material for biomedical applications such as magnetic resonance imaging (MRI), wound dressings, Cartilage replacements, contact lenses, tissue engineering, cell/enzyme immobilization, magnetic field stimulated drug delivery systems, biosensors as well as many other industrial processes.

Acknowledgements

This research work has been done with the financial support of University Grant Commission (UGC), Bangladesh through the Faculty of Engineering, University of Rajshahi. The researchers also acknowledge the supports of Bangladesh Atomic Energy Commission (BAEC) for the permission of using its laboratory facilities.

Conflicts of interest

The authors declare that they have no competing interests.

References

[1] Lu A-H, Salabas EL, Schüth F. Magnetic nanoparticles: synthesis, protection, functionalization, and application. Angew Chemie Int Ed 2007;46:1222–44. http://dx.doi.org/10.1002/anie.200602866.
[2] Pankhurst QA, Connolly J, Jones SK, Dobson J. Applications of magnetic nanoparticles in biomedicine. J Phys D Appl Phys 2003;36:R167–81. http://dx.doi.org/10.1088/0022-3727/36/13/201.
[3] Tadic M, Panjan M, Damnjanovic V, Milosevic I. Magnetic properties of hematite (α-Fe_2O_3) nanoparticles prepared by hydrothermal synthesis method. Appl Surf Sci 2014;320:183–7. http://dx.doi.org/10.1016/j.apsusc.2014.08.193.
[4] Wu W, He Q, Jiang C. Magnetic iron oxide nanoparticles: synthesis and surface functionalization strategies. Nanoscale Res Lett 2008;3:397–415. http://dx.doi.org/10.1007/s11671-008-9174-9.
[5] Tang SCN, Lo IMC. Magnetic nanoparticles: essential factors for sustainable environmental applications. Water Res 2013;47:2613–32. http://dx.doi.org/10.1016/j.watres.2013.02.039.
[6] Baker C, Ismat Shah S, Hasanain S. Magnetic behavior of iron and iron-oxide nanoparticle/polymer composites. J Magn Magn Mater 2004;280:412–8. http://dx.doi.org/10.1016/j.jmmm.2004.03.037.
[7] Novakova AA, Lanchinskaya VY, Volkov AV, Gendler TS, Kiseleva TY, Moskvina MA, et al. Magnetic properties of polymer nanocomposites containing iron oxide nanoparticles. J Magn Magn Mater 2003;258–259:354–7. http://dx.doi.org/10.1016/S0304-8853(02)01062-4.
[8] Gaaz T, Sulong A, Akhtar M, Kadhum A, Mohamad A, Al-Amiery A. Properties and applications of polyvinyl alcohol, Halloysite nanotubes and their nanocomposites. Molecules 2015;20:22833–47. http://dx.doi.org/10.3390/molecules201219884.
[9] Baker MI, Walsh SP, Schwartz Z, Boyan BD. A review of polyvinyl alcohol and its uses in cartilage and orthopedic applications. J Biomed Mater Res Part B Appl Biomater 2012;100B:1451–7. http://dx.doi.org/10.1002/jbm.b.32694.
[10] DeMerlis C, Schoneker D. Review of the oral toxicity of polyvinyl alcohol (PVA). Food Chem Toxicol 2003;41:319–26. http://dx.doi.org/10.1016/S0278-6915(02)00258-2.
[11] Ben Halima N. Poly(vinyl alcohol): review of its promising applications and insights into biodegradation. RSC Adv 2016;6:39823–32. http://dx.doi.org/10.1039/C6RA05742J.
[12] Schulze K, Koch A, Petri-Fink A, Steitz B, Kamau S, Hottiger M, et al. Uptake and biocompatibility of functionalized poly(vinylalcohol) coated superparamagnetic maghemite nanoparticles by Synoviocytes in vitro. J Nanosci Nanotechnol 2006;6:2829–40. http://dx.doi.org/10.1166/jnn.2006.484.
[13] Jiang Y, Schädlich A, Amado E, Weis C, Odermatt E, Mäder K, et al. In-vivo studies on intraperitoneally administrated poly(vinyl alcohol). J Biomed Mater Res Part B Appl Biomater 2010;9999B. http://dx.doi.org/10.1002/jbm.b.31585.
[14] Kaneo Y, Hashihama S, Kakinoki A, Tanaka T, Nakano T, Ikeda Y. Pharmacokinetics and biodisposition of poly(vinyl alcohol) in rats and mice. Drug Metab Pharmacokinet 2005;20:435–42. http://dx.doi.org/10.2133/dmpk.20.435.
[15] Aguiló-Aguayo N, Maurizi L, Galmarini S, Ollivier-Beuzelin MG, Coullerez G, Bertran E, et al. Aqueous stabilisation of carbon-encapsulated superparamagnetic α-iron nanoparticles for biomedical applications. Dalt Trans 2014;43:13764–75. http://dx.doi.org/10.1039/C4DT00085D.
[16] Singh J, Srivastava M, Dutta J, Dutta PK. Preparation and properties of hybrid monodispersed magnetic α-Fe_2O_3 based chitosan nanocomposite film for industrial and biomedical applications. Int J Biol Macromol 2011;48:170–6. http://dx.doi.org/10.1016/j.ijbiomac.2010.10.016.
[17] Kaushik A, Khan R, Solanki PR, Pandey P, Alam J, Ahmad S, et al. Iron oxide nanoparticles–chitosan composite based glucose biosensor. Biosens Bioelectron 2008;24:676–83. http://dx.doi.org/10.1016/j.bios.2008.06.032.
[18] Rinki K, Dutta PK, Dutta J. Chitosan based scaffolds for tissue engineering applications. Asian Chitin J 2007;3:69–78.
[19] Rinki K, Dutta PK. Chitosan based scaffolds by lyophilization and sc.CO 2 assisted methods for tissue engineering applications. J Macromol Sci Part A 2010;47:429–34. http://dx.doi.org/10.1080/10601321003659630.
[20] Tang Z-X, Qian J-Q, Shi L-E. Preparation of chitosan nanoparticles as carrier for immobilized enzyme. Appl Biochem Biotechnol 2007;136:77–96. http://dx.doi.org/10.1007/BF02685940.
[21] Agnihotri SA, Mallikarjuna NN, Aminabhavi TM. Recent advances on chitosan-based micro- and nanoparticles in drug delivery. J Control Release 2004;100:5–28. http://dx.doi.org/10.1016/j.jconrel.2004.08.010.
[22] Hee Kim E, Sook Lee H, Kook Kwak B, Kim B-K. Synthesis of ferrofluid with magnetic nanoparticles by sonochemical method for MRI contrast agent. J Magn Magn Mater 2005;289:328–30. http://dx.doi.org/10.1016/j.jmmm.2004.11.093.
[23] Zigeuner RE, Riesenberg R, Pohla H, Hofstetter A, Oberneder R. Isolation of circulating cancer cells from whole blood by immunomagnetic cell enrichment and unenriched immunocytochemistry in vitro. J Urol 2003;169:701–5. http://dx.doi.org/10.1016/S0022-5347(05)63996-1.
[24] El Sayed AM, Morsi WM. α-Fe2O3/(PVA + PEG) Nanocomposite films; synthesis, optical, and dielectric characterizations. J Mater Sci 2014;49:5378–87. http://dx.doi.org/10.1007/s10853-014-8245-9.
[25] Kavitha A, Prabu HG, Babu SA. Synthesis of low-cost iron oxide: chitosan nanocomposite for antibacterial activity. Int J Polym Mater 2013;62:45–9. http://dx.doi.

org/10.1080/00914037.2012.670816.
[26] Kavitha AL, Subashini A. Synthesis and characterization of iron oxide – chitosan nanocomposite for dye decolourization. J Adv Chem Sci Appl 2015;3:2347–7601.
[27] Guo Z, Zhang D, Wei S, Wang Z, Karki AB, Li Y, et al. Effects of iron oxide nanoparticles on polyvinyl alcohol: interfacial layer and bulk nanocomposites thin film. J Nanoparticle Res 2010;12:2415–26. http://dx.doi.org/10.1007/s11051-009-9802-z.
[28] Wei Y, Zhang X, Song Y, Han B, Hu X, Wang X, et al. Magnetic biodegradable Fe_3O_4/CS/PVA nanofibrous membranes for bone regeneration. Biomed Mater 2011;6:55008. http://dx.doi.org/10.1088/1748-6041/6/5/055008.
[29] Tański T, Matysiak W, Witek P. UV-vis analysis of composite polyacrylonitrile/iron oxide nanoparticles thin fibrous mats. Appl Eng Lett 2017;2:54–9.
[30] Huang K-C, Ehrman SH. Synthesis of iron nanoparticles via chemical reduction with palladium ion seeds. Langmuir 2007;23:1419–26. http://dx.doi.org/10.1021/la0618364.
[31] Akbara S, Hasanaina SK, Azmatb N, Nadeem M. Synthesis of Fe2O3 nanoparticles by new Sol-Gel methodand their structural and magnetic characterizations. arXiv Prepr Cond-mat/0408480 2004.
[32] Mia MNH, Pervez MF, Hossain MK, Reefaz Rahman M, Uddin MJ, Al Mashud MA, et al. Influence of Mg content on tailoring optical bandgap of Mg-doped ZnO thin film prepared by sol-gel method. Results Phys 2017;7:2683–91. http://dx.doi.org/10.1016/j.rinp.2017.07.047.
[33] Mia NH, Rana SM, Pervez F, Rahman MR, Hossain K, Al Mortuza A, et al. Preparation and spectroscopic analysis of zinc oxide nanorod thin films of different thicknesses. Mater Sci 2017;35:501. http://dx.doi.org/10.1515/msp-2017-0066.
[34] Pervez MF, Mia MNH, Hossain S, Saha SMK, Ali MH, Sarker P, et al. Influence of total absorbed dose of gamma radiation on optical bandgap and structural properties of Mg-doped zinc oxide. Optik (Stuttg) 2018;162:140–50. http://dx.doi.org/10.1016/j.ijleo.2018.02.063.
[35] Hossain MK, Ferdous J, Haque MM, Hakim AKMA. Development of nanostructure formation of Fe73.5Cu1Nb3Si13.5B9 alloy from amorphous state on heat treatment. World J Nano Sci Eng 2015;5:107–14. http://dx.doi.org/10.4236/wjnse.2015.54013.
[36] Hossain MK, Pervez MF, Mia MNH, Tayyaba S, Uddin MJ, Ahamed R, et al. Annealing temperature effect on structural, morphological and optical parameters of mesoporous TiO2 film photoanode for dye-sensitized solar cell application. Mater Sci 2017;35:868–77. http://dx.doi.org/10.1515/msp-2017-0082.
[37] Hossain MK, Pervez MF, Uddin MJ, Tayyaba S, Mia MNH, Bashar MS, et al. Influence of natural dye adsorption on the structural, morphological and optical properties of TiO_2 based photoanode of dye-sensitized solar cell. Mater Sci 2018;36. http://dx.doi.org/10.1515/msp-2017-0090.
[38] Hossain MK, Mortuza AA, Sen SK, Basher MK, Ashraf MW, Tayyaba S, et al. A comparative study on the influence of pure anatase and Degussa-P25 TiO_2 nanomaterials on the structural and optical properties of dye sensitized solsr cell (DSSC) photoanode. Optik (Stuttg) 2018. http://dx.doi.org/10.1016/j.ijleo.2018.05.032.
[39] Pascau JBJMMPJ. Image Processing with ImageJ. 2nd ed. Packt Publishing; 2015.
[40] Guo L, Huang Q, Li X, Yang S. Iron nanoparticles: Synthesis and applications in surface enhanced Raman scattering and electrocatalysis. Phys Chem Chem Phys 2001;3:1661–5. http://dx.doi.org/10.1039/b0099511.
[41] Sun Y-P, Li X, Cao J, Zhang W, Wang HP. Characterization of zero-valent iron nanoparticles. Adv Colloid Interface Sci 2006;120:47–56. http://dx.doi.org/10.1016/j.cis.2006.03.001.
[42] Morris MC, McMurdie HF, Evans EH, Paretzkin B, Parker HS, Panagiotopoulos NC. Standard X-ray Diffraction Powder Patterns. Sect. 18, n.d.
[43] Kayani ZN, Arshad S, Riaz S, Naseem S. Synthesis of iron oxide nanoparticles by sol-gel technique and their characterization. IEEE Trans Magn 2014;50:1–4. http://dx.doi.org/10.1109/TMAG.2014.2313763.
[44] Reda SM. Synthesis of ZnO and Fe_2O_3 nanoparticles by sol–gel method and their application in dye-sensitized solar cells. Mater Sci Semicond Process 2010;13:417–25. http://dx.doi.org/10.1016/j.mssp.2011.09.007.
[45] Blaney L. Magnetite (Fe3O4): Properties, Synthesis, and Applications. vol. 15. 2007.
[46] Wang Y-XJ, Hussain SM, Krestin GP. Superparamagnetic iron oxide contrast agents: physicochemical characteristics and applications in MR imaging. Eur Radiol 2001;11:2319–31. http://dx.doi.org/10.1007/s003300100908.
[47] Hossain MK, Ferdous J, Haque MM, Hakim AKMA. Study and characterization of soft magnetic properties of Fe73.5Cu1Nb3Si13.5B9 magnetic ribbon prepared by rapid quenching method. Mater Sci Appl 2015;6:1089–99. http://dx.doi.org/10.4236/msa.2015.612108.
[48] Namduri H, Nasrazadani S. Quantitative analysis of iron oxides using Fourier transform infrared spectrophotometry. Corros Sci 2008;50:2493–7. http://dx.doi.org/10.1016/j.corsci.2008.06.034.
[49] Blout ER, Karplus R. The infrared spectrum of polyvinyl alcohol. J Am Chem Soc 1948;70:862–4. http://dx.doi.org/10.1021/ja01182a504.
[50] Negrea P, Caunii A, Sarac I, Butnariu M. The study of infrared spectrum of chitin and chitosan extract as potential sources of biomass. Dig J Nanomater Biostruct 2015;10:1129–38.
[51] Cano L, Pollet E, Avérous L, Tercjak A. Effect of TiO_2 nanoparticles on the properties of thermoplastic chitosan-based nano-biocomposites obtained by mechanical kneading. Compos Part A Appl Sci Manuf 2017;93:33–40. http://dx.doi.org/10.1016/j.compositesa.2016.11.012.
[52] Hanemann T, Szabó DV. Polymer-nanoparticle composites: from synthesis to modern applications. Materials (Basel) 2010;3:3468–517. http://dx.doi.org/10.3390/ma3063468.
[53] Jeon I-Y, Baek J-B. Nanocomposites derived from polymers and inorganic nanoparticles. Materials (Basel) 2010;3:3654–74. http://dx.doi.org/10.3390/ma3063654.
[54] Xu L, Huang Y-A, Zhu Q-J, Ye C. Chitosan in molecularly-imprinted polymers: current and future prospects. Int J Mol Sci 2015;16:18328–47. http://dx.doi.org/10.3390/ijms160818328.